2016-06

Fluid-structure interaction of channel driven cavity flow

Arceneaux, Stephen M.

Monterey, California: Naval Postgraduate School

NAVAL POSTGRADUATE SCHOOL

MONTEREY, CALIFORNIA

THESIS

FLUID-STRUCTURE INTERACTION OF CHANNEL DRIVEN CAVITY FLOW

by

Stephen M. Arceneaux

June 2016

Thesis Advisor:	Young W. Kwon
Second Reader:	Jarema M. Didoszak

THIS PAGE INTENTIONALLY LEFT BLANK

REPORT DOCUMENTATION PAGE			*Form Approved OMB No. 0704-0188*

1. AGENCY USE ONLY ***(Leave blank)***	**2. REPORT DATE** June 2016	**3. REPORT TYPE AND DATES COVERED** Master's Thesis

4. TITLE AND SUBTITLE FLUID-STRUCTURE INTERACTION OF CHANNEL DRIVEN CAVITY FLOW	**5. FUNDING NUMBERS** N/A
6. AUTHOR(S) Stephen M. Arceneaux	
7. PERFORMING ORGANIZATION NAME(S) AND ADDRESS(ES) Naval Postgraduate School Monterey, CA 93943-5000	**8. PERFORMING ORGANIZATION REPORT NUMBER**
9. SPONSORING /MONITORING AGENCY NAME(S) AND ADDRESS(ES)	**10. SPONSORING / MONITORING AGENCY REPORT NUMBER**

11. SUPPLEMENTARY NOTES The views expressed in this thesis are those of the author and do not reflect the official policy or position of the Department of Defense or the U.S. Government. IRB Protocol number ____N/A____.

12a. DISTRIBUTION / AVAILABILITY STATEMENT Approved for public release; distribution is unlimited	**12b. DISTRIBUTION CODE**

13. ABSTRACT (maximum 200 words)

An experimental setup was developed for channel driven cavity flow in order to study the fluid-structure interaction and provide benchmark data for validation of numerical fluid-structure interaction models. The channel driven cavity flow is a modification from lid-driven cavity flow. To examine the fluid-structure interaction, the bottom side of the cavity is a deformable flat plate. All other boundaries are rigid. The fluid-structure interaction inside the cavity is driven by flow through a thin channel topside of the cavity. Water is used as the fluid. Fluid-structure interaction for different deformable plates during constant flow is quantified using a variety of strain and displacement measurement techniques. To establish suitable boundary conditions for numerical analysis of the experiment, the inlet velocity of the channel driven cavity flow is known. Outlet pressure is constant atmospheric. Numerical results are obtained using ANSYS's CFX and structure analysis.

14. SUBJECT TERMS fluid-structure interaction, channel driven cavity flow, lid-driven cavity flow	**15. NUMBER OF PAGES** 61
	16. PRICE CODE

17. SECURITY CLASSIFICATION OF REPORT	**18. SECURITY CLASSIFICATION OF THIS PAGE**	**19. SECURITY CLASSIFICATION OF ABSTRACT**	**20. LIMITATION OF ABSTRACT**
Unclassified	Unclassified	Unclassified	UU

NSN 7540-01-280-5500

Standard Form 298 (Rev. 2-89)
Prescribed by ANSI Std. 239-18

THIS PAGE INTENTIONALLY LEFT BLANK

Approved for public release; distribution is unlimited

FLUID-STRUCTURE INTERACTION OF CHANNEL DRIVEN CAVITY FLOW

Stephen M. Arceneaux
Ensign, United States Navy
B.S., United States Naval Academy, 2015

Submitted in partial fulfillment of the
requirements for the degree of

MASTER OF SCIENCE IN MECHANICAL ENGINEERING

from the

NAVAL POSTGRADUATE SCHOOL
June 2016

Approved by: Young W. Kwon
Thesis Advisor

Jarema M. Didoszak
Second Reader

Garth V. Hobson
Chair, Department of Mechanical and Aerospace Engineering

THIS PAGE INTENTIONALLY LEFT BLANK

ABSTRACT

An experimental setup was developed for channel driven cavity flow in order to study the fluid-structure interaction and provide benchmark data for validation of numerical fluid-structure interaction models. The channel driven cavity flow is a modification from lid-driven cavity flow. To examine the fluid-structure interaction, the bottom side of the cavity is a deformable flat plate. All other boundaries are rigid. The fluid-structure interaction inside the cavity is driven by flow through a thin channel topside of the cavity. Water is used as the fluid. Fluid-structure interaction for different deformable plates during constant flow is quantified using a variety of strain and displacement measurement techniques. To establish suitable boundary conditions for numerical analysis of the experiment, the inlet velocity of the channel driven cavity flow is known. Outlet pressure is constant atmospheric. Numerical results are obtained using ANSYS's CFX and structure analysis.

THIS PAGE INTENTIONALLY LEFT BLANK

TABLE OF CONTENTS

LIST OF FIGURES

LIST OF TABLES

THIS PAGE INTENTIONALLY LEFT BLANK

ACKNOWLEDGMENTS

I would like to thank Professor Kwon for teaching me the value of starting experiments early and continuing with a steady pace. Professor Colin Ratcliffe at the U.S. Naval Academy instilled in me an interest in signal processing and instrumentation, which was invaluable to this thesis. Finally, I would like to thank Mom and Dad for ensuring I received the best education possible while I lived at home.

THIS PAGE INTENTIONALLY LEFT BLANK

I. INTRODUCTION

A. BACKGROUND

Simple case physical experiment data for a fluid-structure interaction problem is needed to validate numerical models of fluid-structure interaction. One such fluid mechanics problem is lid-driven cavity flow. In lid-driven cavity flow, the top surface of a cavity moves at a specified velocity and the fluid motion is then solved. Lid-driven cavity flow is complex due to vortices that develop in the center and corners of the cavity. Figure 1 displays the boundary conditions for lid-driven cavity flow.

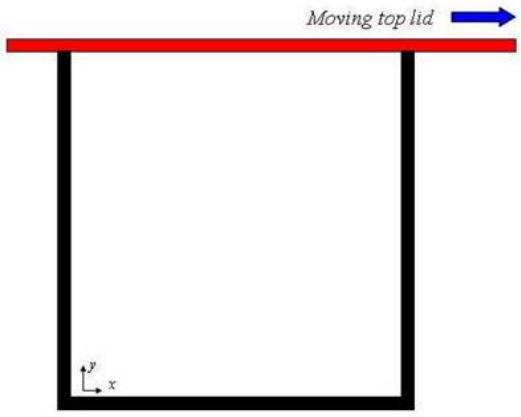

Figure 1. Two-Dimensional Lid Cavity Flow Boundary Conditions. Source: [1].

In practice, however, lid-driven cavity flow is difficult to simulate in an experiment. Various methods—such as using a belt to act as the moving lid—have been tested and met with varying degrees of success. One such attempt is performed by Liberzon [2], in which a belt drove fluid flow in a cubic cavity. However, this experiment, shown in Figure 2, only analyzed fluid flow and not fluid-structure interaction.

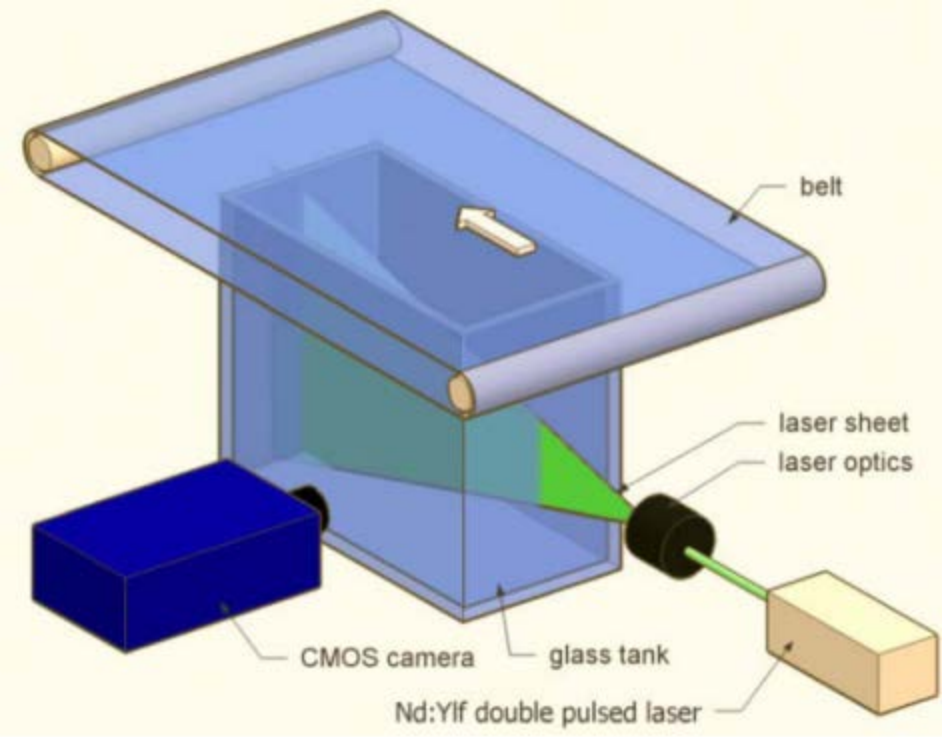

Figure 2. Lid-driven Cavity Flow Belt Drive. Source: [2].

To the author's best knowledge, experimental data for the fluid-structure interaction problem of lid-driven cavity flow has never been published. Thus, this thesis provides benchmark data for the validation of a numerical fluid-structure interaction solution.

B. OBJECTIVES

The objectives of this thesis are:

1. Perform a numerical study for fluid-structure interaction of channel driven cavity flow.
2. Construct a physical model and conduct experiments providing benchmark data for fluid-structure interaction of channel driven cavity flow.

C. METHODOLOGY

Due to the complex nature of previous experimental setups, such as belt drives to simulate lid-driven cavity flow, a new approach was considered. This approach is referred to as channel driven cavity flow. In channel driven cavity flow, a cavity exists

under a thin channel of moving fluid. The inlet and exit channels are long enough so that the fluid flow is fully developed as the channel flow interacts with the cavity flow. The inlet velocity is known and the outlet is an opening into the atmosphere. Thus, atmospheric pressure is maintained at the outlet. This experiment setup provides constant and robust boundary conditions.

The effect of a thin channel of fluid driving the cavity flow is similar enough to that of belt driven flow, which, while it ideally simulates lid-driven cavity flow when working correctly, was deemed too unreliable for this experiment. However, the numerical model should be constructed with channel driven flow and not with a moving lid.

THIS PAGE INTENTIONALLY LEFT BLANK

II. EXPERIMENTAL SETUP FOR CHANNEL DRIVEN CAVITY FLOW

The design and fabrication of the experimental apparatus and data acquisition techniques are discussed. The experimental apparatus was constructed of acrylic so the fluid motion could be observed. A flow meter, strain gages, digital image correlation, and laser displacement sensors quantified parameters of the experiment.

A. DESIGN AND FABRICATION

The fluid volume dimensions were chosen to provide a large enough space for the cavity flow to develop into a swirling vortex and for the inlet and outlet flow profiles to become fully developed. Figure 3 shows the volume occupied by the fluid. The dimensions of the experimental fluid volume are available in the Appendix.

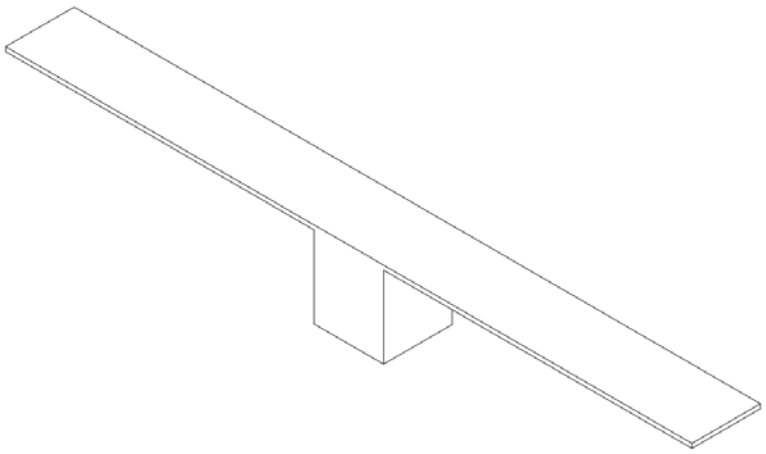

Figure 3. Fluid Volume.

A structure made of clear acrylic was designed to contain the fluid volume and provide a flat deformable plate boundary. A schematic of this structure is shown in Figure 4.

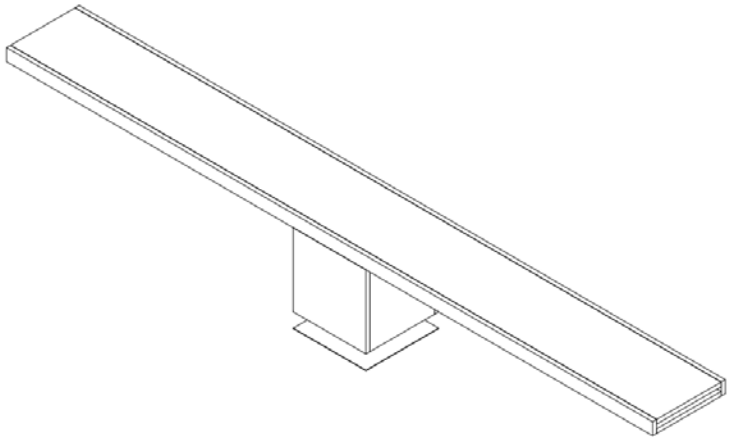

Figure 4. Acrylic Structure with Flat Plate Separated from the Structure for Viewing.

1. Acrylic Channel Cavity Structure

The channel cavity structure was manufactured using acrylic sheets bonded together first with SCIGRIP 16 Fast Set clear, medium-bodied solvent cement and second with SCIGRIP 4 Fast Set clear, water-thin solvent cement. First, the two acrylic sheets were oriented so that a clamping force could be applied to hold the parts together. Wooden beams were laid between the clamps and the acrylic so that the pressure was distributed more evenly and the solvent cement would be distributed evenly across the bond. Uneven pressure resulted in gaps in the bond in which the cement could not fill. Figure 5 displays the clamping technique used to bond the acrylic sheets.

Figure 5. Clamping Technique.

To apply the 16 solvent cement, a bead was laid on the acrylic sheet interface using the provided tube of cement. Then, the parts were put together and the clamping force applied. Once the cement cured, the parts were structurally stable enough to support the load of both handling and experiment operation. However, the bond was not yet watertight.

To make the bond watertight, the parts were clamped together after the 16 solvent cement cured. Then, the 4 solvent cement was applied across the corner of the joint and the thin cement entered the bond due to capillary action, which was capable due to the gaps in the bond. Finally, a bead of 16 solvent cement was applied along the joint, similar to the plumbing technique of caulking a sink or bathtub. The structure was now watertight. During experiment operation, the acrylic structure bonds had no detectable leaks. The completed acrylic structure is shown in Figure 6.

Figure 6. Acrylic Structure.

2. Other Design Considerations

A large trough holds a reservoir of water that feeds the channel driven flow structure. A constant flowrate pump circulated the water through the channel. The flowrate was controlled by two valves. One valve controlled the flow of water directly back to the reservoir. The other valve controlled the flow of water through the channel cavity structure. A GPI TM Series water meter measured flow rate accurate to one hundredth of a gallon per minute.

In order to create an adapter to connect the circular pipe from the pump outlet and the rectangular channel inlet, a rubber adapter was constructed using 2.4 mm ($\frac{3}{32}$") thick neoprene rubber sheet. The sheet was bonded to the acrylic using 3M Scotch-Weld Neoprene High Performance Rubber and Gasket Adhesive 1300. A bead of 100% silicone was applied on the bond to prevent water from infiltrating the adhesive. The 3M Scotch-Weld 1300 adhesive kept the neoprene bonded to the acrylic while the silicone prevented water from leaking. A securing strap was placed around the neoprene that was bonded to the acrylic channel to prevent the pressure from breaking the seal during operation. The neoprene sheet was folded around the channel and another sheet of neoprene sealed the seam, acting as a patch. The neoprene patch was bonded to the neoprene adapter with 3M Scotch-Weld 1300. A bead of AQUASEAL Urethane Repair

Adhesive & Sealant was applied at the bond-water interface to prevent water from leaking and compromising the adhesive. Finally, the neoprene adapter was secured with hose clamps around the pipe that supplied water. 3M Scotch-Weld 1300 adhesive and silicone were applied on the pipe-neoprene interface to prevent leaks.

Inside the neoprene adapter, a honeycomb cell was bonded to the channel inlet in order to smooth the flow entering the channel and help achieve fully developed flow as quickly as possible in the channel.

The performance of this adapter was astounding. After minor adjustments, there were no leaks. Liberal application of silicone and adhesive is critical to ensuring the adapter performs as designed.

B. DATA ACQUISITION SYSTEMS

Strain gages, digital image correlation cameras, and laser displacement sensors quantified strain and displacement of the flat deformable plate during fluid-structure interaction.

1. Strain

Strain data was acquired using Micro-Measurements bi-directional strain gages, National Instruments NI9945, NI9215, and NI cDAQ-9174 Hardware, and National Instruments Signal Express software. The sampling frequency used was 1,000 Hz. Figure 7 displays a bi-directional strain gage.

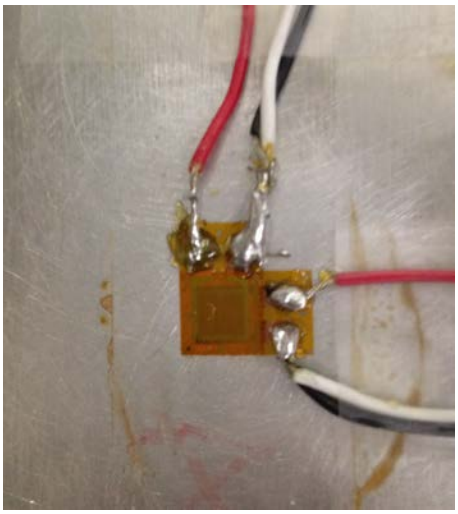

Figure 7. Bi-Directional Strain Gage.

2. Digital Image Correlation

The digital image correlation technique uses two cameras in a stereo orientation to produce a three-dimensional deformation field of a surface. Figure 8 shows the cameras used.

Figure 8. Digital Image Correlation Cameras.

To create a speckle pattern on the surface, which is required for digital image correlation, the specimen—in this case, the flat deformable plate—was painted white and then black paint was “flicked” onto the specimen using a hard bristle brush. Figure 9 shows a finished speckle pattern. The red lines and numbers are dimension measurements used to align the plate in the experiment.

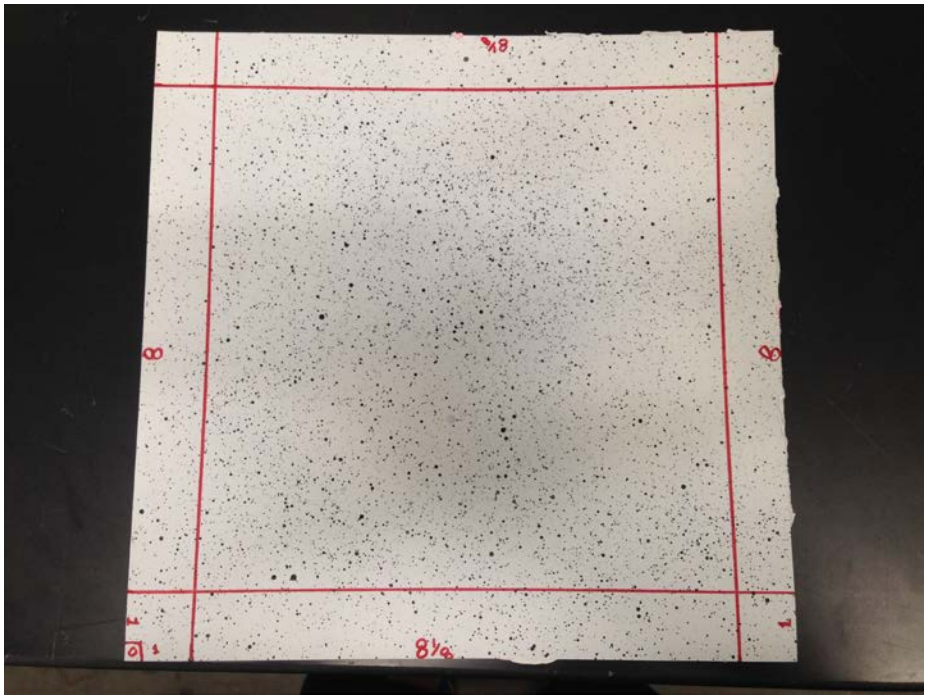

Figure 9. Speckle Pattern on the Deformable Plate.

There must be a high-intensity light source for the correlation software to adequately map the whole image captured by the cameras. A low-intensity light source produced an inconsistent deformation plot in which large areas of the specimen had no discernable deformation data. Increasing the light intensity corrected this problem. In Figure 10, the displacement plot breaks down at approximately -35 mm in the x-direction due to inadequate lighting.

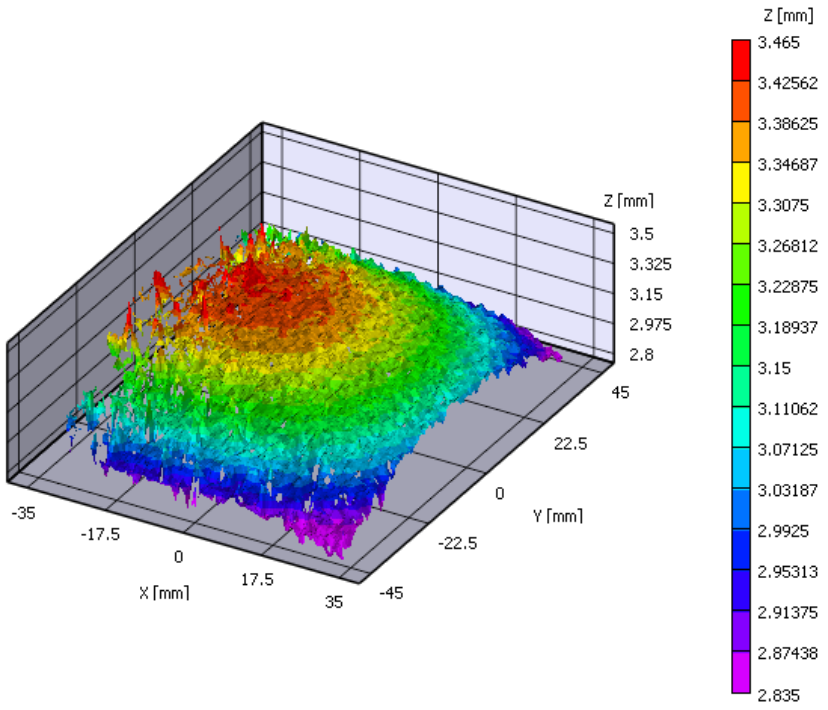

Figure 10. Incomplete Deformation Plot.

3. Laser Displacement Sensor

Laser displacement sensors measured the displacement of the plate at certain points on the deformable flat plate. A Keyence IL-030 sensor head and Keyence amplifier unit measured displacement and output a voltage corresponding to the displacement. Then, a National Instruments NI 9215 voltage measurement module and National Instruments Signal Express software measured and logged the voltage. The sampling frequency used was 1,000 Hz. The IL-030 laser sensor head is shown in Figure 11 with the laser seen in the bottom of the image. The sensor head measures the distance of the laser beam, so the sensor head was set up so that the laser beam was perpendicular to the deformable plate to measure accurate displacement.

Figure 11. Laser Displacement Sensor Head.

C. EXPERIMENTAL PROCEDURES

In order to be able to replicate the experiment as a numerical fluid-structure interaction model, suitable boundary conditions must be specified.

1. Boundary Conditions

To solve the fluid model, inlet uniform velocity and exit pressure were chosen as boundary conditions. Inlet velocity is variable and measured with a flowmeter. The channel exit is an opening to the atmosphere. Thus, the exit pressure boundary condition is constant atmospheric. Inlet velocity and exit pressure provide enough boundary conditions to solve the fluid model. Figure 12 shows the experimental apparatus. Note that the fluid outlet on the left hand side of the image empties into the black reservoir.

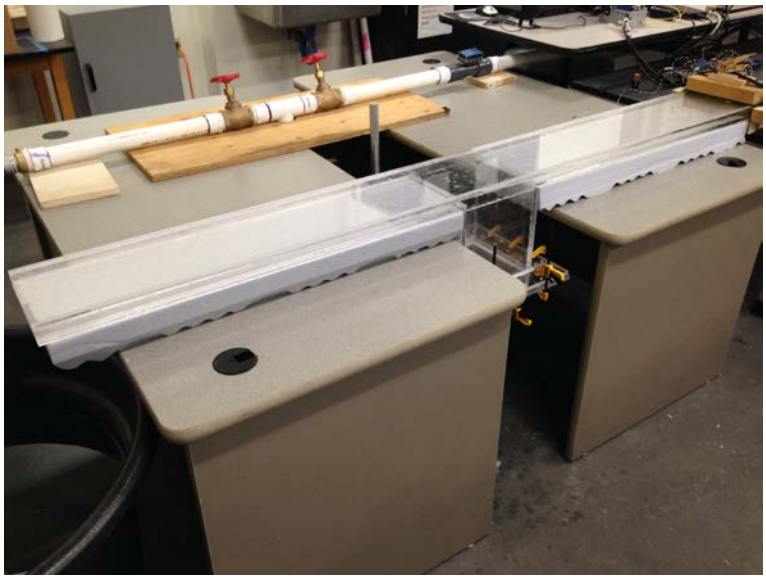

Figure 12. Experiment Apparatus.

The deformable flat plate boundary conditions are clamped on all edges. A clamped boundary condition specifies zero slope and zero displacement at the edges of the plate. Figure 13 shows the cavity with the clamped boundary conditions of the deformable plate.

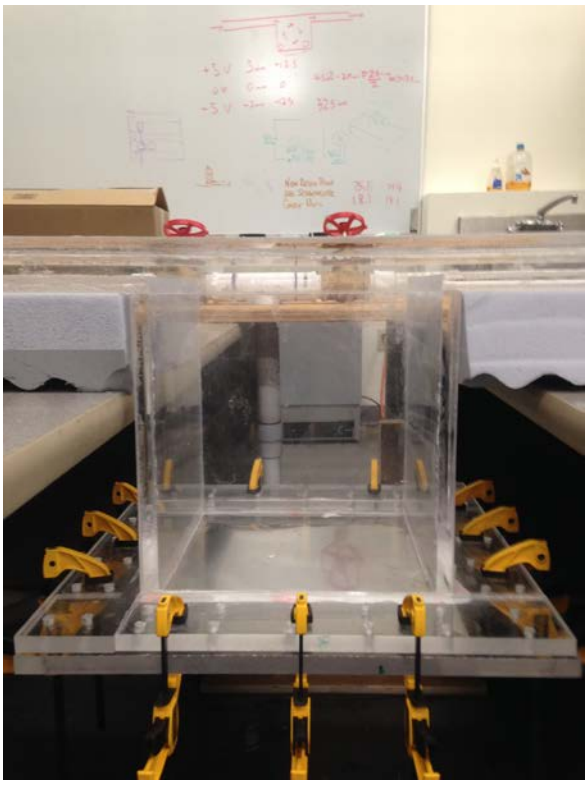

Figure 13. Cavity with Clamped Boundary Conditions of Plate.

2. Deformable Plate Material Selection

Aluminum alloy 6061-T6 of thickness 0.5 mm (0.02”) and 1.0 mm (0.04”) and 302 stainless steel of thickness 0.13 mm (0.005”) were considered for analysis because of their availability. Digital image correlation revealed that the stainless steel warped during pressure loading and was not suitable for the experiment. The aluminum plates did not show detectable warping. Figure 14 shows the warping of the steel plate during constant pressure loading from a static water column.

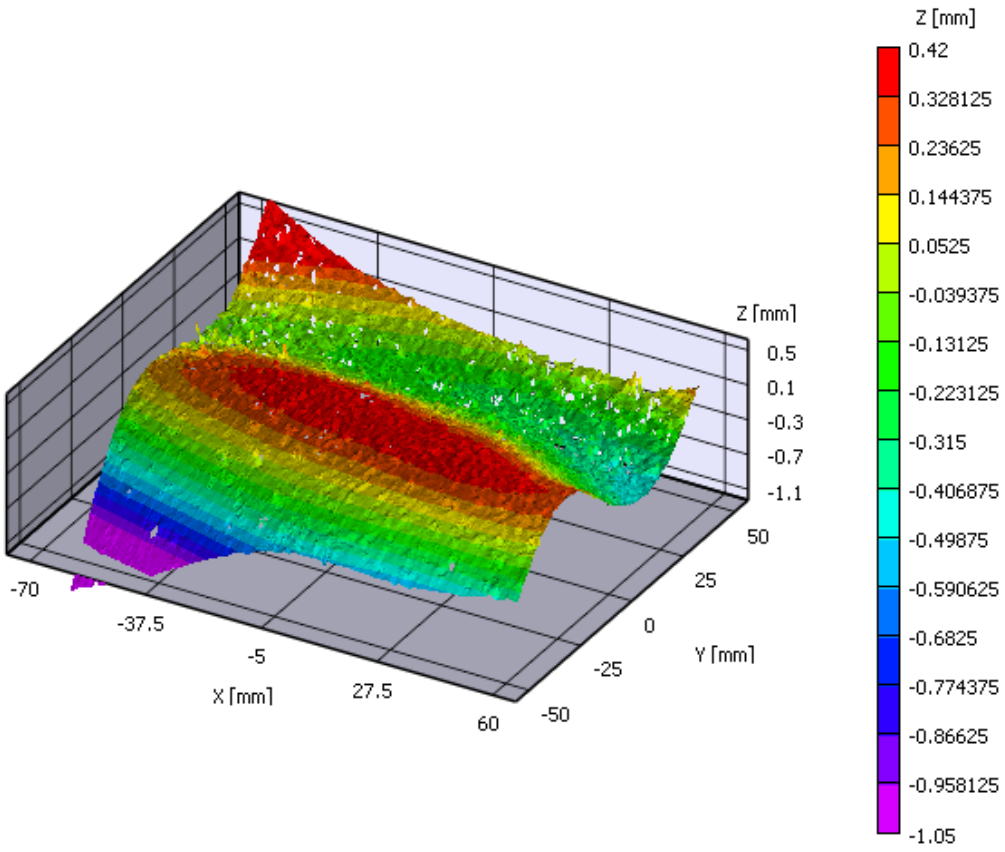

Figure 14. Warping Deformation of Stainless Steel.

III. NUMERICAL RESULTS AND DISCUSSION

A. PLATE BENDING

In order to determine if the experimental data could be used to verify a numerical model without the need for normalized data, analytical and numerical analyses of the flat plate were conducted for simple test cases of constant pressure loading. If the analytical and numerical solutions matched the experimental data, then the data could be used as is for verification of fluid-structure interaction models.

1. Numerical Analysis of the Flat Plate

An aluminum plate of dimensions 203 mm x 206 mm (8" x 8⅛"), the same dimensions as the experiment plate, was modeled in ANSYS using a two dimensional quadrilateral mesh of 2550 (approximately 50 x 50 elements). Fixed supports were applied at the plate edges consistent with the clamped boundary conditions in the physical experiment.

a. Static Deflection of Plate Subjected to Fluid Pressure

The height of the static water column in the cavity with no water flow is 240 mm ($9\frac{7}{16}$"). This water produces a uniform pressure of 2,348 Pa on the plate. For the numerical study, the pressure was varied from 0 Pa to 4,000 Pa in increments of 200 Pa. 4,000 Pa was selected as the maximum pressure because ANSYS CFX predicts a maximum pressure below 4,000 Pa when fluid is flowing through the channel at the pump's maximum flowrate. A parametric study was conducted for the 0.5 mm (0.02") and 1.0 (0.04") thick aluminum plates using both linear deflection and non-linear, large deflection models on each plate. Figure 15 displays the results of the study.

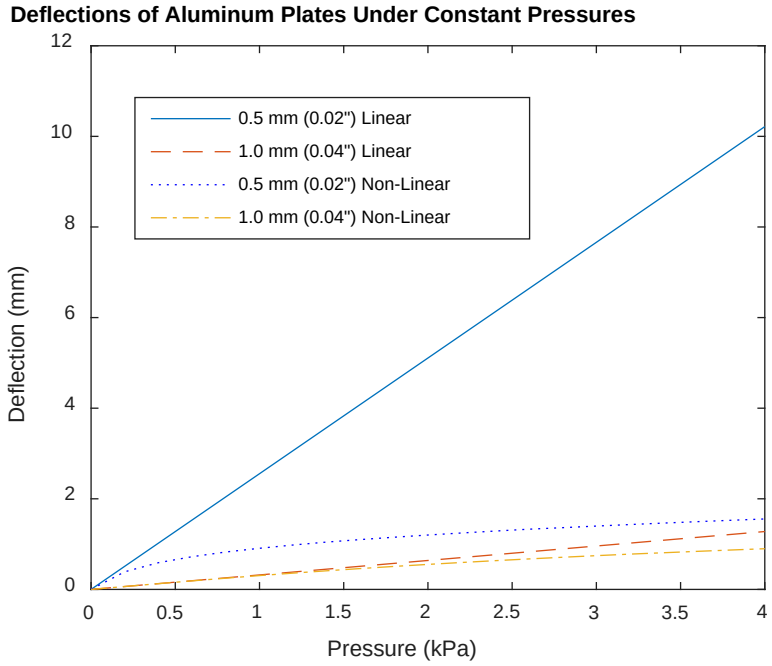

Figure 15. Deflection of Aluminum Plates.

The parametric study shows that, for the range of pressures expected in the experiment, the 1.0 mm (0.04”) plate has similar behavior for the linear and non-linear, large deflection models. The 0.5 mm (0.02”) plate, however, has drastic differences. This result means that the 1.0 mm (0.04”) thick aluminum plate will be able will be able to be modeled in the linear elastic region and produce similar results to the physical experiment.

b. Modal Analysis

The natural frequencies of the 0.5 mm (0.02”) thick aluminum plate, with the same dimensions as the experiment plate and no damping, were found in order to determine if any modes of vibration would be excited during experiment operation. The natural frequencies of the plate predicted by ANSYS’s modal analysis are shown in Table 1.

Table 1. Natural Frequencies of the 0.5 mm (0.02”) Thick Aluminum Plate

Mode	Frequency (Hz)
1	107
2	217
3	222

The 1.0 mm (0.04”) thick plate frequencies were not determined because they are known to be higher than the 0.5 mm (0.02”) thick plate. During the experiment, none of the 0.5 mm (0.02”) thick plate frequencies were excited. The frequency content existed only in the 0-10 Hz range. Even with water backed damping, it was assumed that the plate natural frequency was still out of this range.

2. Analytical Analysis of Flat Plate

Published approximate solutions for the deformation and mode frequency of a flat plate were used to validate the numerical solutions. These solutions assume the plate is deforming in the linear elastic region only and do not account for non-linear effects. The analytical solutions match the linear elastic numerical solutions very closely and provide proof of accuracy.

a. Deformation under Constant Load

Timoshenko [3] provides a solution for the maximum deflection of a rectangular square plate with Poisson’s ratio of 0.3. Although the experimental plate of 0.5 mm (0.02”) thickness is approximately square with dimensions of 203 mm x 206 mm (8” x 8⅛”) and is made of T6-6061 aluminum with an approximate Poisson’s ratio of 0.33, the error due to these slight variations was assumed negligible. Equation 1 is Timoshenko’s solution. L is the plate side length, D is the plate rigidity, and q is the pressure loading.

$$w_{\max} = 0.00126q\frac{L^4}{D} \tag{1}$$

When calculating plate rigidity using a Poisson’s ratio of 0.33, Equation 1 results in a maximum displacement of 6.1 mm.

Piley [4] provides a solution for the maximum displacement of a plate dependent on length, width, and Poisson's ratio. Equations 2 and 3 are used to determine the constant used in the displacement solution. Using Equation 4, the maximum displacement of the plate is calculated. The maximum displacement using Piley's solution is 6.0 mm.

$$\alpha = \frac{L_x}{L_y} \tag{2}$$

$$c_1 = -0.06479 + 0.1327\alpha - 0.0665\alpha^2 + 0.01162\alpha^3 \tag{3}$$

$$w_{\max} = c_1 q \frac{L^4}{Eh^3} \tag{4}$$

b. Modal Analysis

Piley [4] offers an approximate solution for the natural frequencies of a plate with clamped boundary conditions. Using Equations 5 and 6, a constant is calculated to determine the natural frequency. Equation 7 results in the natural frequency in units of rad/s. Equation 8 converts the answer to Hertz. Piley's solution results in a first mode frequency of 107 Hz which his consistent with the ANSYS solution shown in Table 1. The first mode occurs when maximum displacement occurs at the center only.

$$\beta = \frac{L_x}{L_y} \tag{5}$$

$$\lambda_1 = \beta^2(89.3 - 84.73\beta + 36.7\beta^2 - 5.27\beta^3) \tag{6}$$

$$\omega_1 = \frac{\lambda_1}{L^2}\sqrt{\frac{D}{\rho}} \tag{7}$$

$$f_1 = \frac{\omega_1}{2\pi} \tag{8}$$

B. CHANNEL DRIVEN CAVITY FLOW

The channel driven cavity flow fluid-structure interaction was modeled using ANSYS's CFX and structural analysis in order to determine if the experimental results would match a numerical solution. The fluid volume was meshed using rectangular elements and a maximum element sizing specified so that at least 10 elements existed in the channel height. This maximum element size was maintained throughout the whole

fluid volume. The transient fluid motion clearly shows a vortex in which the center circulates in the cavity.

1. Transient Fluid Analysis with Rigid Plate

The fluid motion was analyzed using all rigid wall boundaries around the fluid volume. A uniform inlet velocity of 1 m/s was used. 1 m/s is within the range of velocities the physical experiment can produce. The outlet was specified as an opening with constant atmospheric pressure. A time step of 0.1 seconds was used for the transient analysis and the fluid started from rest. Figures 16, 17, and 18 show the fluid velocity streamlines at different time steps. Each image is a view of the side of the cavity, looking at the no slip wall boundary. This analysis was three dimensional, but the images selected show only one side of the three dimensional cavity. There is a vortex that begins in the upper right-hand quadrant of the fluid volume and travels around the cavity in a clockwise motion.

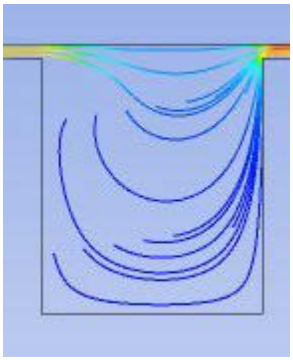

Figure 16. Streamlines at 0.1 Seconds. Inlet on the Left, Outlet on the Right.

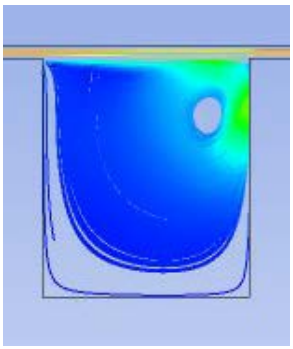

Figure 17. Streamlines at 0.8 Seconds. Inlet on the Left, Outlet on the Right.

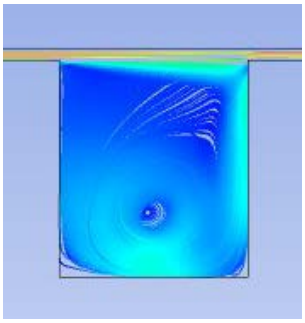

Figure 18. Streamlines at 2.4 Seconds. Inlet on the Left, Outlet on the Right.

2. One-Way Pressure Field Transfer Fluid-Structure Interaction

To simulate the effects of fluid-structure interaction, a one-way pressure field transfer model was created. This model calculates the pressure along the interface of the deformable flat plate and then transfers the pressure to a static structural solver which will calculate the deflection of the plate. The effects of the plate geometry and change in the fluid volume geometry due to deflection were assumed to be negligible for this analysis, so a one-way analysis was used. A more accurate analysis would involve a two way fluid-structure interaction approach in which the updated geometry due to plate deflection is transferred to the fluid volume and the mesh geometry is changed. For this solution, an inlet velocity of 1.22 m/s was chosen because it can be replicated in the physical experiment. Although the mesh size was not consistent between the fluid analysis and solid plate analysis, ANSYS automatically interpolates the solution to fit the mesh. When a 0.5 mm (0.02”) thick aluminum plate was used, a strain of 769 microns

was shown to exist in the center of plate in the direction of fluid flow. This strain can be compared to the experimental data.

THIS PAGE INTENTIONALLY LEFT BLANK

IV. EXPERIMENTAL RESULTS AND DISCUSSION

A. DIGITAL IMAGE CORRELATION

The digital image correlation technique proved suitable for quantifying static displacement of the flat deformable plate for a specific experiment trial. The frame rate of the cameras was at maximum 6 frames per second and was not fast enough to capture the motion of the plate, which oscillated within a frequency band of approximate 0-10 Hertz. Figure 19 displays the deflection of the 0.5 mm (0.02”) thick aluminum plate under constant pressure load from the water column of the cavity with reference to no pressure. The cameras were unable to capture the whole plate so the center (maximum) of the plate was chosen for view. A maximum 2.01 mm displacement was measured. This measured displacement differed when the plate was remounted another time and measured with the laser displacement sensor. Digital image correlation was abandoned due to its inability to capture images at a suitable frame rate and the inconsistencies in displacements between experiment runs due to the variance in boundary conditions when the plate was clamped to the structure.

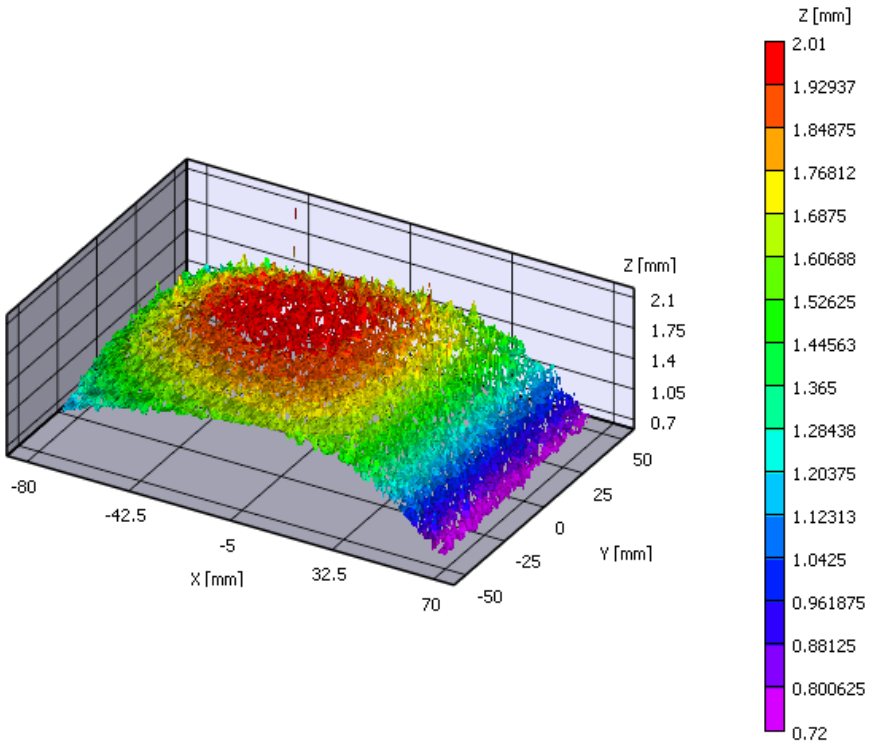

Figure 19. Aluminum Displacement.

B. STRAIN GAGES

Strain data for the 1.0 mm (0.04”) thick plate was measured at the locations shown in Figure 20. The points chosen were the center and then two off-set points 51 mm (2”) away from the center. The off-set was in the direction of fluid-flow.

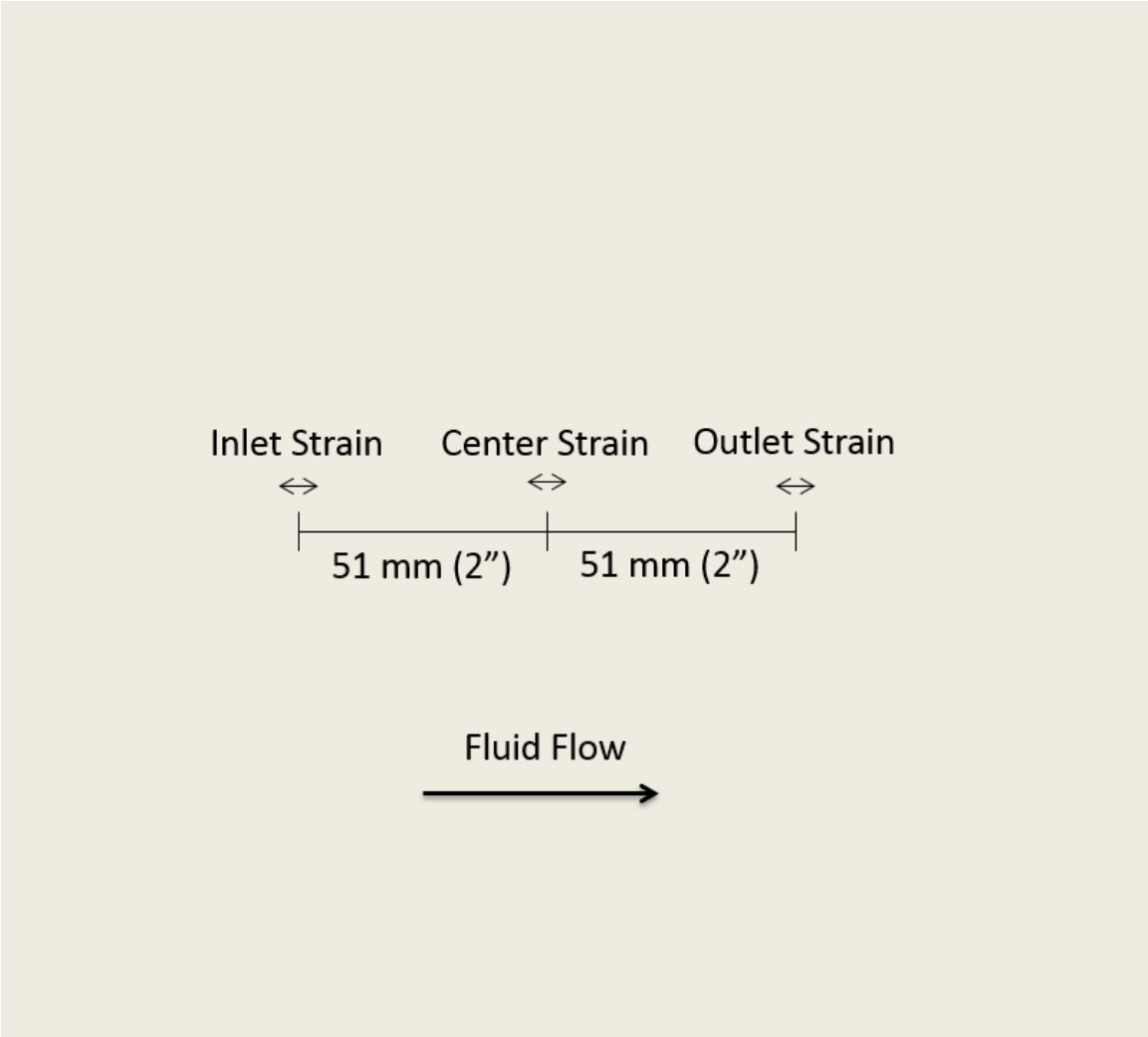

Figure 20. Strain Locations.

Many attempts were made to match the ANSYS numerical solution for a simple case of constant pressure loading to the experimental strain data for constant pressure loading. However, no attempts were close enough for analysis. Possible reasons for error include variations in plate thickness, plate properties, and the experiment boundary condition which ideally should be perfectly clamped but in practice was not. To compensate, the normalized strain data is presented. Equation 9 is the normalized strain at a point *i*. The static strain was measured when the acrylic structure was full of fluid but no fluid motion occurred. The strain is offset by the static strain at the specified point and then normalized by the static center strain. Figure 21 displays the mean normalized strains for certain inlet velocities. Table 2 displays the resulting values.

$$\varepsilon_{i,normalized} = \frac{\varepsilon_i - \varepsilon_{i,static}}{\varepsilon_{center,static}} \tag{9}$$

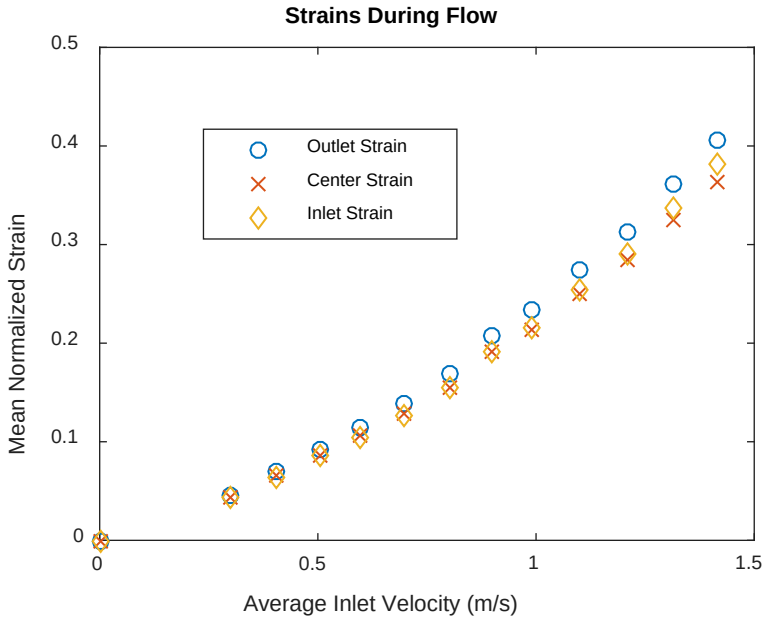

Figure 21. Mean Normalized Strains.

Table 2. Mean Normalized Strains.

Inlet Velocity (m/s)	Outlet	Center	Inlet
0.00	0.0000	0.0000	0.0000
0.30	0.0457	0.0438	0.0434
0.40	0.0699	0.0658	0.0648
0.50	0.0918	0.0863	0.0850
0.60	0.1146	0.1066	0.1046
0.70	0.1380	0.1285	0.1270
0.80	0.1680	0.1558	0.1554
0.90	0.2071	0.1906	0.1914
0.99	0.2337	0.2139	0.2164
1.10	0.2741	0.2499	0.2533
1.21	0.3136	0.2839	0.2913
1.31	0.3610	0.3253	0.3380
1.41	0.4059	0.3636	0.3819

The mean absolute deviation of the strain gage data was computed. The results are displayed in Figure 22. Table 3 shows the resulting values.

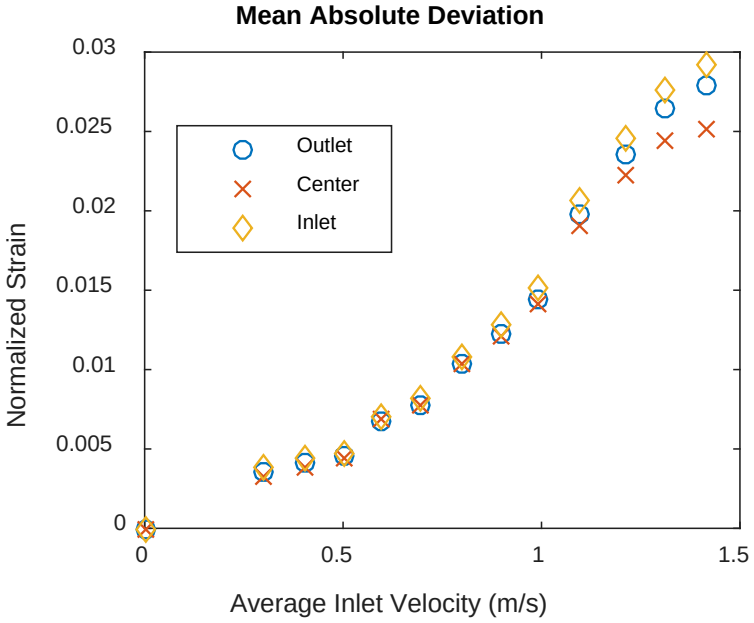

Figure 22. Mean Absolute Deviation of Strains.

Table 3. Mean Absolute Deviation of Strains.

Inlet Velocity (m/s)	Outlet	Center	Inlet
0.00	0.0000	0.0000	0.0000
0.30	0.0036	0.0033	0.0038
0.40	0.0041	0.0039	0.0044
0.50	0.0045	0.0044	0.0048
0.60	0.0068	0.0068	0.0071
0.70	0.0078	0.0078	0.0082
0.80	0.0103	0.0103	0.0108
0.90	0.0123	0.0122	0.0129
0.99	0.0145	0.0141	0.0151
1.10	0.0198	0.0190	0.0206
1.21	0.0236	0.0223	0.0246
1.31	0.0265	0.0244	0.0277
1.41	0.0278	0.0252	0.0291

The normalized center strain response for an average inlet velocity of 1.41 m/s is shown in Figure 23. The mean strain and mean absolute deviation are also shown in the Figure 23.

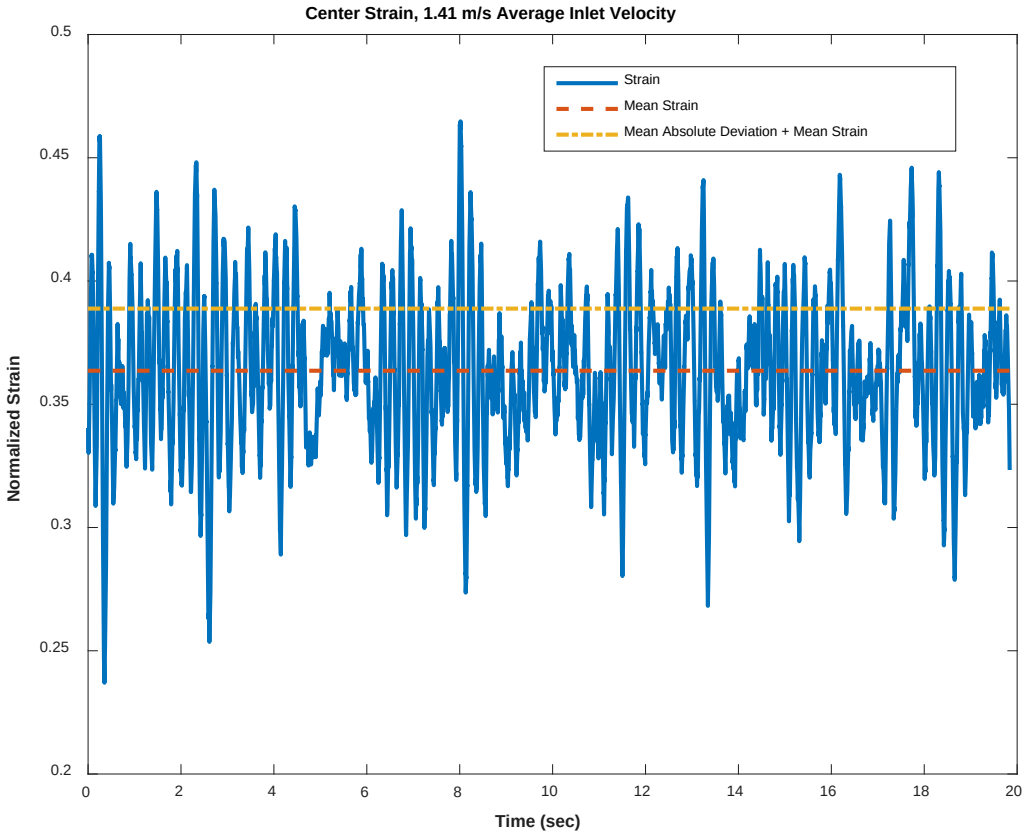

Figure 23. Strain Time History.

C. LASER DISPLACEMENT SENSOR

Displacement was measured at two points, the center strain location and outlet strain location shown in Figure 20. The normalizing procedure for strain at a point *i* was repeated with the displacement data as shown in Equation 10. Because the displacement sensors were mounted to the ground, the deflection of the acrylic structure due to the weight of the water was used as an offset to find the deflection of the plate.

$$d_{i,normalized} = \frac{d_i - d_{i,static}}{d_{center,static}} \tag{10}$$

1. 1.0 mm (0.04”) Thick Aluminum Plate

The mean displacements and mean absolute deviation of the displacement time history were computed for data from the 1.0 mm (0.04”) thick aluminum plate. Figure 24 displays the mean normalized displacements for different inlet velocities. The data presented in Figure 24 appears to be inaccurate because the outlet displacement is greater than center displacement. However, these are normalized displacements and thus the static displacement at each point effects the normalized displacement. Due to the nature of the flow, the pressure distribution will not be uniform across the plate during flow. Thus, the outlet point of measurement has a larger difference between the static displacement and displacement during flow and thus a larger normalized displacement. The data shown in Figure 24 is tabulated in Table 4.

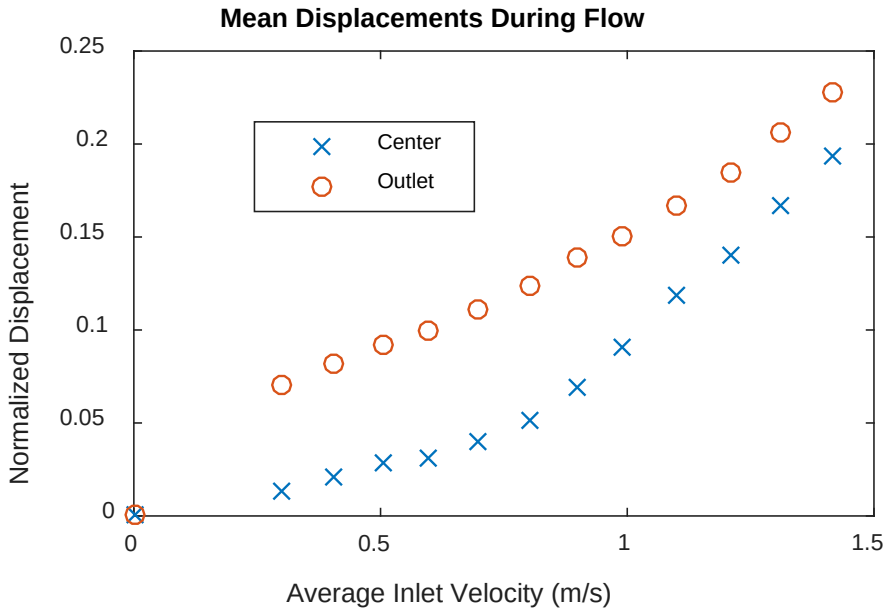

Figure 24. Mean Normalized Displacements of the 1.0 mm (0.04”) Thick Plate.

Table 4. Mean Normalized Displacements of the 1.0 mm (0.04”) Thick Plate.

Inlet Velocity (m/s)	Outlet	Center
0.00	0.0000	0.0000
0.30	0.0702	0.0127
0.40	0.0816	0.0210
0.50	0.0919	0.0283
0.60	0.1000	0.0311
0.70	0.1108	0.0398
0.80	0.1234	0.0517
0.90	0.1388	0.0688
0.99	0.1502	0.0905
1.10	0.1674	0.1188
1.21	0.1842	0.1402
1.31	0.2067	0.1675
1.41	0.2278	0.1931

The same procedure for calculating the normalized strain mean absolute deviation was repeated for displacement. Figure 25 displays the mean absolute deviation from the mean normalized displacement for different inlet velocities. The values are tabulated in Table 5.

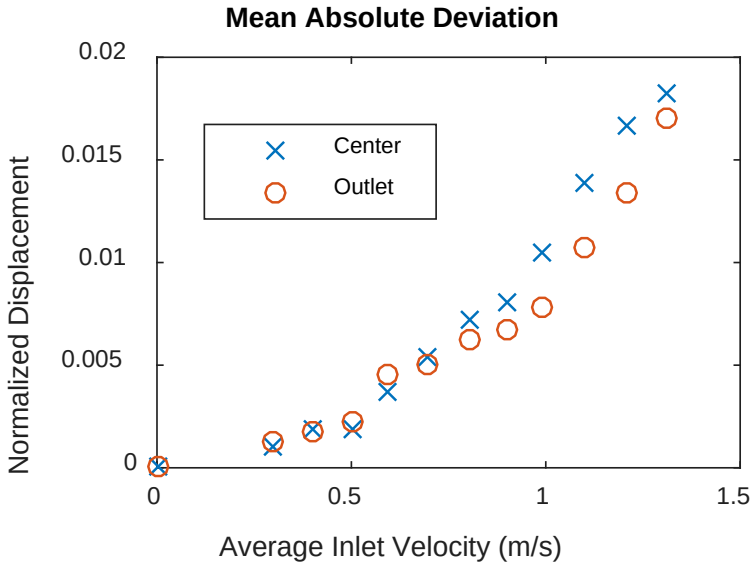

Figure 25. Mean Absolute Deviation from Mean Displacement of the 1.0 mm (0.04”) Thick Plate.

Table 5. Mean Absolute Deviation from Mean Displacement of the 1.0 mm (0.04”) Thick Plate.

Inlet Velocity (m/s)	Outlet	Center
0.00	0.0000	0.0000
0.30	0.0012	0.001
0.40	0.0017	0.0019
0.50	0.0022	0.0019
0.60	0.0046	0.0037
0.70	0.0050	0.0054
0.80	0.0063	0.0072
0.90	0.0068	0.0081
0.99	0.0078	0.0105
1.10	0.0107	0.0138
1.21	0.0134	0.0166
1.31	0.0170	0.0182

2. 0.5 mm (0.02”) Thick Aluminum Plate

The same data processing procedure used for the 1.0 mm (0.04”) thick aluminum plate displacement was repeated on data for the 0.5 mm (0.02”) thick aluminum plate. Figures 26 and 27 display the mean normalized displacements and mean absolute deviations, respectively. The resultant values are tabulated in Tables 6 and 7. Unlike the 1.0 mm (0.04”) mean normalized displacements in which the outlet normalized displacement was greater in magnitude than the center displacement for the range of flowrates, the 0.5 mm (0.02”) plate behaves oppositely. Figure 26 shows that the center mean normalized displacement is greater in magnitude. This behavior is due to the increased flexibility of the plate. The 0.5 mm (0.02”) will have a larger gradient of deflection for a given pressure.

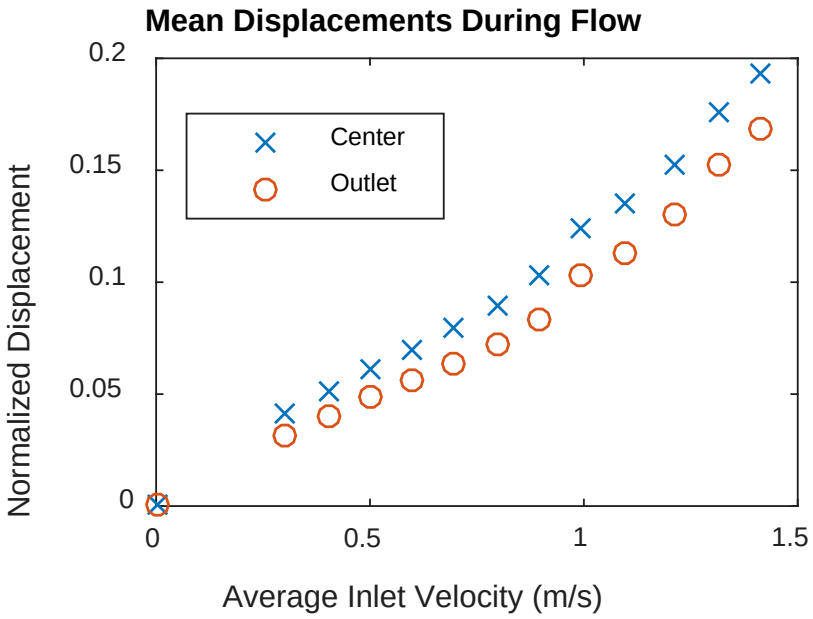

Figure 26. Mean Normalized Displacements of the 0.5 mm (0.02”) Thick Plate.

Table 6. Mean Normalized Displacements of the 0.5 mm (0.02”) Thick Plate.

Inlet Velocity (m/s)	Outlet	Center
0.00	0.0000	0.0000
0.30	0.0315	0.0412
0.40	0.0398	0.0514
0.50	0.0482	0.0614
0.60	0.0561	0.0702
0.70	0.0637	0.0790
0.80	0.0723	0.0894
0.90	0.0835	0.1032
0.99	0.1032	0.1245
1.10	0.1133	0.1347
1.21	0.1300	0.1529
1.31	0.1526	0.1763
1.41	0.1681	0.1936

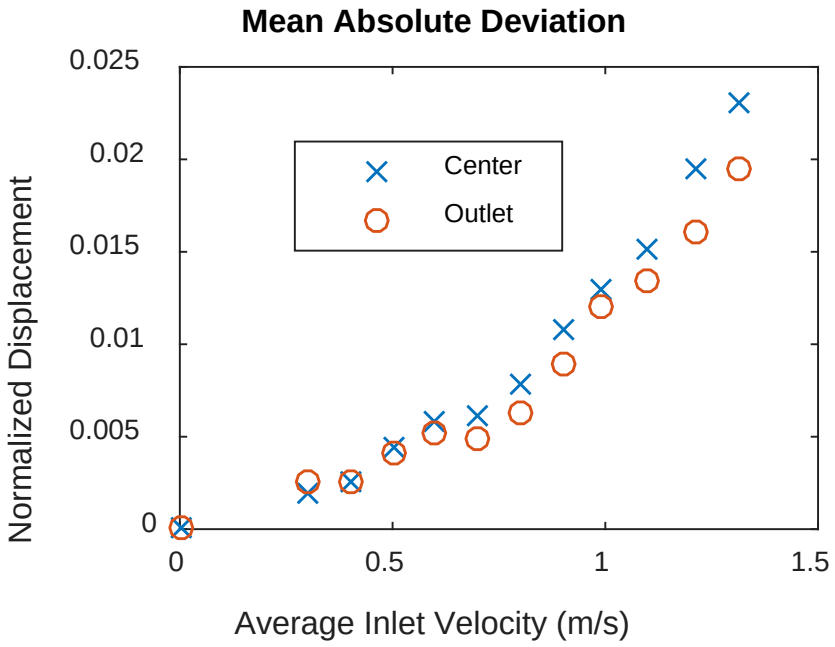

Figure 27. Mean Absolute Deviation from Mean Displacement of the 0.5 mm (0.02") Thick Plate.

Table 7. Mean Absolute Deviation from Mean Displacement of the 0.5 mm (0.02") Thick Plate.

Inlet Velocity (m/s)	Outlet	Center
0.00	0.0000	0.0000
0.30	0.0025	0.0019
0.40	0.0026	0.0026
0.50	0.0042	0.0045
0.60	0.0053	0.0058
0.70	0.0050	0.0061
0.80	0.0062	0.0078
0.90	0.0090	0.0108
0.99	0.0120	0.0129
1.10	0.0134	0.0152
1.21	0.0161	0.0195
1.31	0.0196	0.0230

D. COMPARISON OF NUMERICAL AND EXPERIMENTAL DATA

Many attempts were made to match the numerical and analytical solutions to the experimental data. However, no attempts were considered close enough to assert that the experimental data could be compared directly to a numerical model using the material properties specified in the experiment. Thus, the normalized data was presented to account for errors in plate thickness, plate material properties, and the plate boundary condition. The experimental plate boundary condition is not perfectly clamped. The plate will have a small change in slope at the edges in the physical experiment.

E. UNSTEADY NATURE OF CHANNEL DRIVEN CAVITY FLOW

A numerical model of this physical experiment will most likely predict a steady, cyclic patter to the strain and displacement measurements that were presented in this work. However, the experimental data did not show any type of repeatability in the temporal domain. The nature of the flow must be unsteady and random. The analysis was extended to 20 seconds during steady state flow and the time history of both strain and displacement appeared random. Thus, the mean values and deviations from the mean were presented to provide a useful benchmark for a numerical model that will predict steady, cyclic flow.

THIS PAGE INTENTIONALLY LEFT BLANK

V. CONCLUSION AND FURTHER WORK

A. CONCLUSION

Normalized plate motion data for the channel driven cavity fluid-structure interaction experiment was presented to provide benchmark proof of accuracy data for numerical fluid-structure interaction models. The normalized data was chosen due to the disagreement between numerical solutions for simple cases such as constant pressure loading of a flat plate. These disagreements were due to variances between ideal experiment conditions for material properties and plate boundary conditions and the actual experiment boundary conditions. The numerical fluid solutions did provide, however, a prediction of the pressure distribution on the plate during fluid motion which aided in analysis of the experimental results. Numerical models will most likely predict a steady, cyclic fluid motion and resulting structure response. However, the physical experiment demonstrated unsteady plate motion. Thus, the time history of the strain and displacement was not presented. Instead, the mean value and mean absolute deviation were presented to provide a useful benchmark for a steady, cyclic numerical solution.

B. FUTURE WORK

Different materials, both metals and composites, should be tested to determine their fluid-structure interaction. Specifically, the plate rigidity for a dense metal plate and lighter composite plate should be matched as closely as possible to determine differences for composites in fluid-structure interaction. A transient analysis of the plate should be conducted in which the fluid starts from rest and then accelerates to steady state motion. Attempts should still be made to match the experimental data to analytical and numerical data for the plate strain and deflection for simple cases such as constant pressure loading from static water pressure.

THIS PAGE INTENTIONALLY LEFT BLANK

APPENDIX. FLUID DOMAIN DIMENSIONS

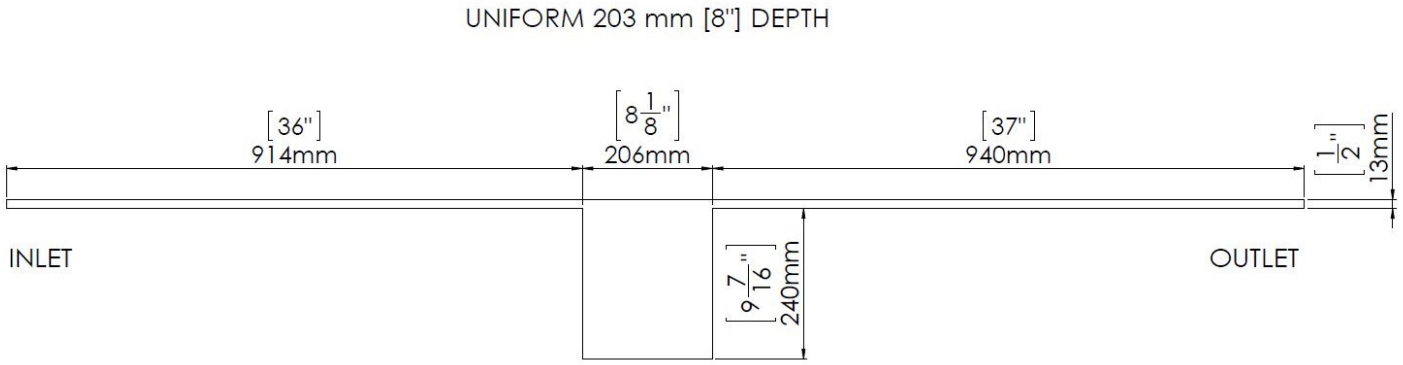

THIS PAGE INTENTIONALLY LEFT BLANK

LIST OF REFERENCES

[1] Laminar flow in a 2-D lid-driven cavity. (n.d.). Nenes Research Group. [Online]. Available: http://nenes.eas.gatech.edu/CFD/1phase/PCCAV1/PCcav.htm. Accessed: Jun. 9, 2016.

[2] A. Liberzon et al., "Experimental observation of the steady—Oscillatory transition in a cubic lid-driven cavity," *Physics of Fluids*, vol. 23, p. 084106-2, 2011. doi: 10.1063/1.3625412

[3] S. Timoshenko and S. Woinowsky-Krieger, *Theory of Plates and Shells*, Second Edition. New York: McGraw-Hill, 1959, ch. 6, sec. 44, p. 202.

[4] W. D. Piley, *Formulas for Stress, Strain, and Structural Matrices*. New York: John Wiley & Sons, 1994, pp. 1042–1050, 1058–1060.

THIS PAGE INTENTIONALLY LEFT BLANK

INITIAL DISTRIBUTION LIST

1. Defense Technical Information Center
   Ft. Belvoir, Virginia

2. Dudley Knox Library
   Naval Postgraduate School
   Monterey, California